Structure-Based Enhanced Capacitance: In Situ Growth of Highly Ordered Polyaniline Nanorods on Reduced Graphene Oxide Patterns

*Mianqi Xue, Fengwang Li, Juan Zhu, Hang Song, Meining Zhang, and Tingbing Cao**

A novel method is described for fabricating an all-solid-state flexible micro-supercapacitor. The microelectrodes of the supercapacitor are prepared by in situ electrodeposition of polyaniline (PANI) nanorods on the surface of reduced graphene oxide (rGO) patterns that are fabricated by micromolding in capillaries. The morphologies of PANI nanorods could be controlled by the concentration of aniline and the growth time in the electrodeposition process. The micro-supercapacitor possesses electrochemical capacitance as high as 970 F g^{-1} at a discharge current density of 2.5 A g^{-1}, as well as good stability, retaining 90% of its initial capacitance after 1700 consecutive cycles for the synergistic effect of these new rGO/PANI nanostructures. The results show that the method could represent a route for translating the interesting fundamental properties of rGO and conducting polymers into technologically viable energy devices. Furthermore, this study might further guide the preparation of functional graphene-based materials.

1. Introduction

Rapid developments of modern digital life mean that new electrode materials are required for energy storage devices to improve their performance. These materials need high power density, moderate energy density, good operational safety, and long cycling life as well as low cost and environmental friendliness. In recent years, numerous research groups in both academia and industry around the world have consciously increased efforts to meet the coming generation of energy storage.[1] Since the first successful fabrication of a graphene-based supercapacitor in 2006,[2] nanocomposite electrode materials based on reduced graphene oxide (rGO)[2–8] and other active materials have attracted great interest. rGO, a competitive alternative to graphene, has the advantages of the properties of graphene while being easier to fabricate.[9,10] It has been shown that, due to their high specific surface area and excellent conductivity, rGO-based materials perform well in electrodes and as current collectors in solar cells,[11] secondary batteries,[12] and especially supercapacitors.[13–18] As one of the ideal electrode materials, rGO-based materials are only restricted by unsatisfactory capacitance performance (generally 100–200 F g^{-1})[14,15] because the capacitance of rGO depends on the electrical double layer at the interface between electrode and electrolyte. On the other hand, compared with rGO-based materials, conducting polymers show much higher capacitance due to the pseudocapacitance of the redox reactions of the electrode material,[18–23] but they are limited by the poor cycle life for practical applications in supercapacitors, which could be complemented by rGO. Therefore, researchers are striving to integrate rGO-based materials and conducting polymers into devices to get satisfactory electrochemical performance, including high capacitance and good cycle life.[16,24,25]

Normally, the structure of electrode materials is the crucial issue determining their energy storage performances. Various methods have been explored to design new structures of electrode materials with good electrochemical performance. For rGO and conducting polymers, they have been developed from the solution mixing of disordered conducting-polymer nanorods[26,27] to electrochemical growth of ordered composite materials,[28,29] or in situ polymerization in solution.[30] It has been reported that the capacitance and stability of electrode materials can be improved by increasing the degree of order, which can bring synergistic effects as well as high surface area and shortening of the ionic-diffusion path.[1e] Unfortunately, the performance of rGO layers and conducting polymer nanorods in existing advanced composites are still restricted by their disorder on the macro scale. For example, in the latest work by Xu and co-workers,[29] despite a large improvement in cycle life, GO-based synergistic composite materials still lack the most effective ionic-diffusion path due to the separation of conductive polymers between each graphene oxide sheet. It remains a great challenge to fabricate highly ordered conducting-polymer-nanorod arrays on large-scale continuous rGO electrodes for energy-storage devices.

Here, we report a solution-based method that allows uniform and controllable in situ electrochemical growth of conducting polyaniline (PANI) nanorod arrays on patterned rGO thin films with thickness of around 20 nm over large areas. Highly ordered PANI nanorod arrays are vertically grown on flat rGO patterns, making them potentially useful in nanoelectronics

M. Xue, F. Li, J. Zhu, H. Song, Dr. M. Zhang, Prof. T. Cao
Department of Chemistry
Renmin University of China
Beijing 100872, P. R. China
E-mail: tcao@chem.ruc.edu.cn

DOI: 10.1002/adfm.201101989

© 2012 WILEY-VCH Verlag GmbH & Co. KGaA, Weinheim

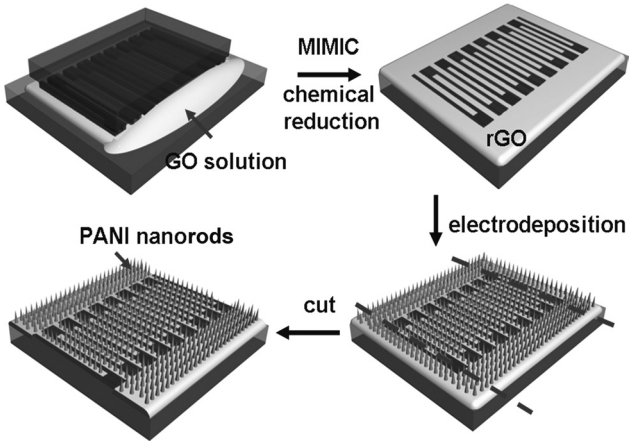

Figure 1. Fabrication of rGO/PANI microelectrodes.

and energy storage. Inspired by the notable effort by Liu and coworkers,[30b] who proposed a facile and easily scalable strategy for a lightweight and flexible ultrathin all-solid-state supercapacitor, we used nanocomposites of PANI nanorod arrays on rGO patterns to fabricate an all-solid-state flexible micro-supercapacitor. The specific capacitance of the nanocomposites in the device can reach as high as 970 F g^{-1} at a discharge current density of 2.5 A g^{-1} (the specific capacitance of PANI nanorods in these composites is as high as 1268 F g^{-1}) which is at the same level as the highest specific capacitance in other reported rGO/PANI composites.[28–30] In addition, the cycle life of these composites is much better than those of PANI nanorod arrays on patterned gold electrodes (after 1700 consecutive cycles, rGO/PANI composites retained 90% of their initial capacitance, while gold/PANI was shown to decrease quickly to 80% after less than 500 cycles).

2. Results and Discussion

2.1. Fabrication of rGO/PANI Microelectrodes

Figure 1 shows the procedure used to fabricate rGO/PANI microelectrodes, which is based on the micromolding in capillary (MIMIC) method[31] and electrodeposition. Firstly, the interdigital finger patterns of continuous rGO electrodes were achieved on a flexible polydimethylsiloxane (PDMS) substrate by the MIMIC method with GO aqueous solution, and then the patterned GO was chemically reduced with hydrazine vapor.[32] PANI nanorod arrays were prepared by performing potentiostatic electrochemical growth with rGO electrode patterns impregnated with a solution of aniline (0.05 M) and H_2SO_4 (0.5 M). The potential of rGO electrodes was firstly fixed at 0.75 V versus Ag/AgCl reference electrode and then kept constant while the current changed with time. In this procedure, the adsorbed aniline monomers on the surface of the graphene patterns were electropolymerized to form rGO/PANI nanocomposites. The rGO/PANI interdigital fingers were then made by cutting along the dashed line on the surface as shown in Figure 1.

In the MIMIC process, the morphologies of the GO patterns are determined by the patterns on the PDMS surface. In our design, they were set at 20 μm for easy fabrication of centimeter-long continuous patterns[33] —the appropriate scale for application in micro-supercapacitors. Meanwhile, the length of the GO patterns is only determined by the channels in the PDMS stamp while the thickness can be easily controlled by adjusting the concentration of GO solution used in MIMIC. After hydrazine-vapor reduction, the obtained rGO patterns show similarity in film morphology and thickness to the original GO pattterns. The optical images (**Figure 2**a,b) show the obtained large-area, centimeter-long, aligned rGO interdigital fingers on a PDMS stamp. There are some dark colored dots in the optical images, which arise from the aggregation of rGO during the solution process. Furthermore, at the end of each finger electrode, there are defects caused by the closed channel used in the MIMIC process, which is shown in the ellipses on Figure 2b. Atomic force microscopy (AFM) images (Figure 2c,d) show the perfect continuous surface of rGO and some stacked rGO sheets. The thickness of the patterned rGO films is ca. 15–30 nm. The specific surface area of the rGO used to electrodeposit PANI nanorods was 142 m^2 g^{-1}.

Figure 3a shows the Raman spectrum of the rGO patterns. Micro-Raman spectroscopy (532 nm) was taken on a single

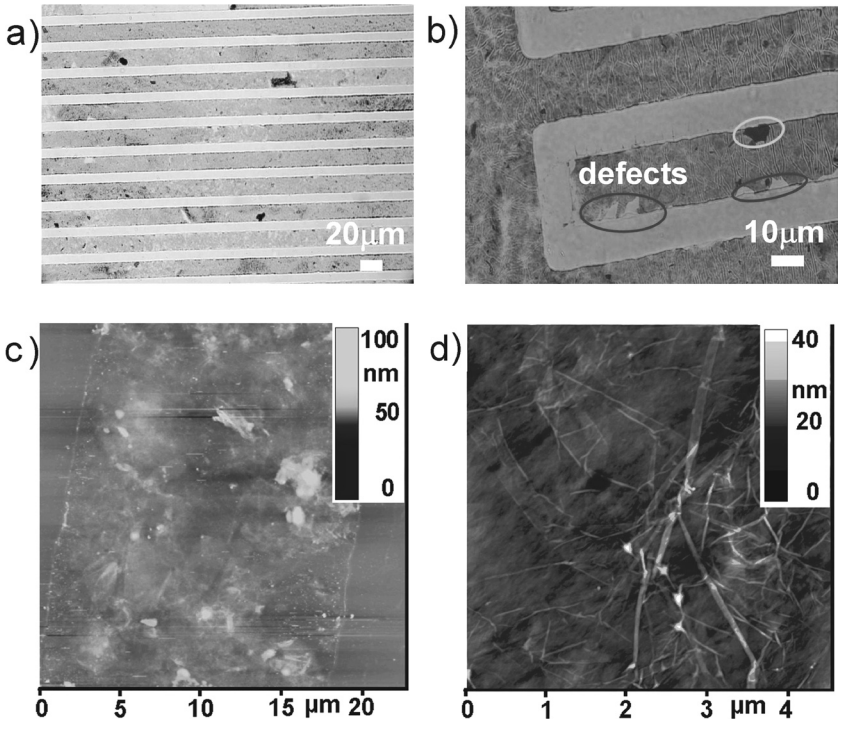

Figure 2. a) Optical image of patterned rGO electrodes (dark lines) on PDMS stamp. b) Optical image of the end of interdigital fingers. c) AFM image of patterned rGO on PDMS stamp and the magnified view (d).

© 2012 WILEY-VCH Verlag GmbH & Co. KGaA, Weinheim

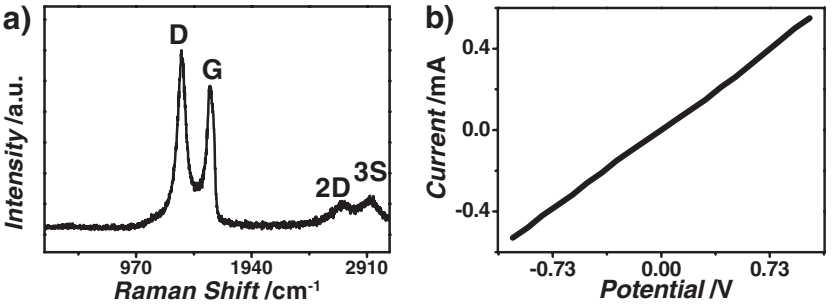

Figure 3. a) Raman spectrum of the rGO patterns showing the D band at 1349 cm^{-1}, the G band at 1594 cm^{-1}, the 2D band at 2700 cm^{-1}, and the S3 peak at 2939 cm^{-1}. b) Linear *I–V* curves with potential from –1 to 1 V on rGO electrodes.

finger of the pattern directly at room temperature. As shown in the spectrum resulting from the PDMS substrate, D and G peaks are observed at ≈1349 and ≈1594 cm^{-1}. The G peak corresponds to the E_{2g} mode observed for sp^2 carbon domains, while the D peak indicates edges and/or defects of the sp^2 domains. Moreover, the D and G bands in the ratio expected for rGO are similar to previously reported Raman spectra of hydrazine-reduced GO films.[8] Figure 3b shows the linear current–voltage (*I–V*) curves on rGO electrodes. Two stylus electrodes were used to investigate the conductance of the resulting rGO patterns on PDMS. As shown in the figure, the obtained rGO patterns are electrically continuous, exhibiting ohmic behavior. The large resistance (2 kΩ for ≈0.2 cm long rGO patterned electrode) is likely due to the remaining defects on the rGO sheets and the scattering effects arising from the rGO stacking, which is in agreement with a previous report for the rGO nanosheets.[34] Additionally, the rGO electrodes, with dense space between layers and good physical adsorption onto the PDMS stamp, ensure that the subsequent electrochemical growth occurs only on the surface layer of rGO patterns.

Figure 4a,b shows the scanning electron microscope (SEM) images of the rGO/PANI composites after electrochemical growth on the rGO electrode patterns with a growth time of about 4500 s. The morphologies of rGO/PANI inherit the structure of rGO electrodes but possess dense vertical nanorod arrays. As shown in Figure 4b, the dense PANI nanorod arrays on the rGO surface are about 20 nm in diameter measured by SEM and about 100–200 nm in height (as shown in Figure S1 in the Supporting Information). In a parallel experiment, gold interdigital finger electrodes with the same feature of rGO patterns were used for electrochemical growth of PANI nanorod arrays. The gold microelectrodes (with thickness of 20 nm) were fabricated by nanotransfer printing.[35] High-magnification SEM images (Figure 4b,d) indicate that the rGO/PANI composites exhibit a similar morphology to the PANI nanorod arrays on gold interdigital finger electrodes after 4500 s growth, but with smaller diameter and smoother surface. Moreover, the differences become more obvious with time, as shown in Figure S2 in the Supporting Information. The whisker-like PANI nanostructures on rGO or gold are similar to other reported results of PANI/GO, rGO/PANI and PANI on a nonporous carbon monolith.[36] Comparison of the SEM results shows that the use of patterned rGO electrodes for PANI growth allows the growth to be better controlled than when gold electrodes are used. Remarkably, such rGO/PANI composites with novel structure can result in a flexible composite electrode with some advantages, such as (i) improved electrical conductivity between PANI and rGO for in situ growth, (ii) homogeneous ion accessibility and large surface area for uniform and slim PANI nanorod arrays, and (iii) a synergistic effect[1a,22,23,37] supercapacitive storage mechanism that will greatly impact the electrochemical performance of energy devices, as shown later (electric double-layer charging/discharging and pseudocapacitive redox reactions of PANI layers).

Raman spectroscopy and SEM were used to study the growth process of PANI on rGO interdigital finger electrodes. The growth rate mainly depends on the concentration of monomer and the conductivity of rGO electrodes. After the growth rate is determined, the morphology of PANI can be controlled by adjusting the growth time. The rGO surface is not yet fully covered by PANI nanorod arrays (as shown in **Figure 5**a) after 2000 s, so the Raman spectrum shows the representative peaks arising from both rGO and PANI, but mainly from rGO. As shown in Figure 5b, a new representative peak arising from

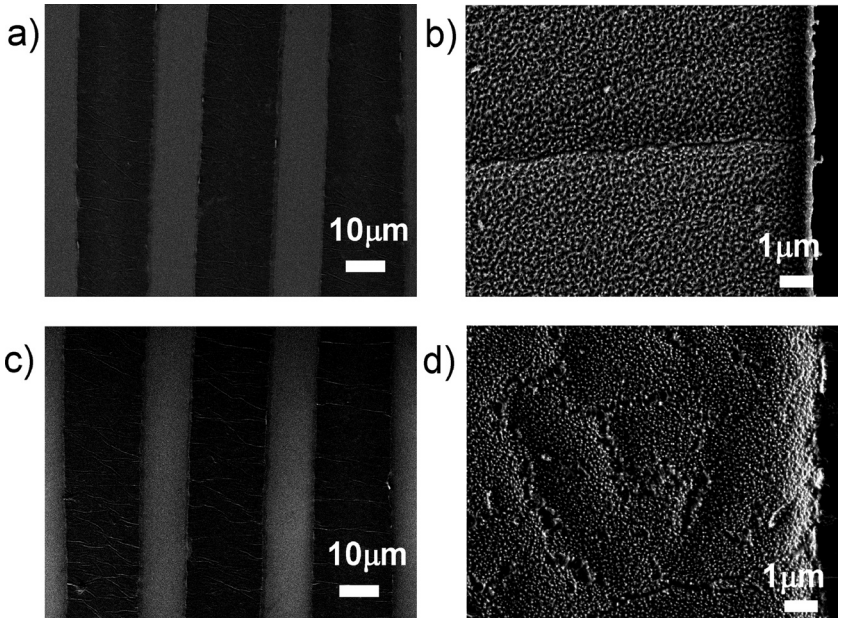

Figure 4. SEM images of PANI nanorods on rGO pattern (a,b) and on gold electrodes (c,d). Panels (a) and (c) are low-magnification SEM images while (b) and (d) are high-magnification SEM images.

© 2012 WILEY-VCH Verlag GmbH & Co. KGaA, Weinheim

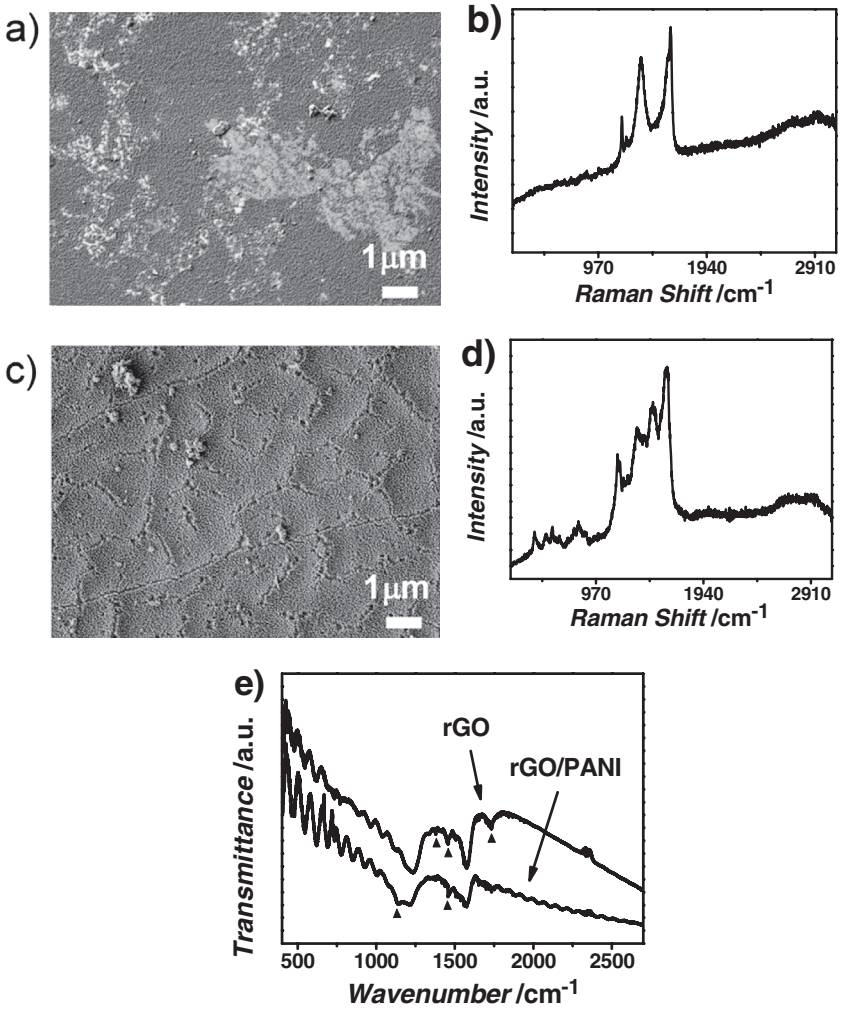

Figure 5. SEM images, Raman spectra, and Fourier transform infrared (FTIR) spectra show the electrochemical growth of PANI nanorod arrays on the rGO surface. a,b) The SEM image and Raman spectrum show the partially rGO/PANI composites covered surface. c,d) The SEM image and Raman spectrum show the densely rGO/PANI composites covered surface. e) FTIR spectra of rGO patterns and rGO/PANI composites on PDMS substrates.

PANI can be indexed at 1170 cm^{-1}; apart from the D/G bands of rGO patterns, another representative peak arising from PANI can be indexed at 1624 cm^{-1}, emerging in the image with the enhancement of the G peak from rGO. After about 5000 s (current response recorded during electropolymerization is shown in Figure S3 in the Supporting Information), the rGO surface is densely covered with PANI nanorod arrays (as shown in Figure 5c), and the Raman spectrum shows the full features of PANI. The peaks at 1165 and 1470 cm^{-1} correspond to C–H vibrations in the quinoid/phenyl groups and the semiquinone radical cation structure in PANI, respectively.[38,39] The intensities of the Raman peaks associated with PANI increase as the electrochemical growth continues, indicating the gradual polymerization of PANI. Thus, we can control the morphology of PANI nanorod arrays, including the length and diameter of single nanorods and the surface roughness of rGO/PANI composites, by adjusting the previously mentioned conditions.

To further verify the composition of PANI and rGO, we measured the IR spectra of the products. As shown in Figure 5e, for the rGO sample, the characteristic vibrations include the weak C=O peak in the carboxylic acid and carbonyl moieties at 1730 cm^{-1}, the C–OH peak at 1368 cm^{-1}, the C–N peak at 1309 cm^{-1}, the C–O–C peak at 1243 cm^{-1}, the C–O stretching peak at 1065 cm^{-1}, and the aromatic C–H peak at 830 cm^{-1}. All these weak peaks can be attributed to the residual chemically active defect sites, which render rGO a promising material for electrochemical growth of conducting polymer nanorod arrays.[29] For the rGO/PANI composites sample, the weak C=O peak of the carboxylic acid carbonyl moieties at 1730 cm^{-1} and the C–OH peak at 1368 cm^{-1} disappear, which is consistent with the electrochemical polymerization and covalent bonding between PANI and rGO. It is also clear that the spectrum of the rGO/PANI composites sample presents the C=C stretching deformation of the benzenoid rings around 1490 cm^{-1}, and the enhanced peak at 1160 cm^{-1} corresponds to C=N stretching, which also suggests that PANI can be successfully deposited on the rGO surface. In comparison, the FTIR spectrum of the rGO/PANI composites sample illustrates the obvious presence of PANI characteristic vibrations, suggesting PANI had been successfully deposited on the GO surface.

2.2. rGO/PANI Nanocomposites for Energy Storage

Figure 6 shows representative cyclic voltammograms (CVs) for the gold/PANI electrode (Figure 6a) and rGO/PANI electrode (Figure 6b) at scan rates of 10, 20, 50, 100, and 200 mV s^{-1} in 1 M Na_2SO_4 recorded in the potential range of –0.2 and 1 V, respectively. A pair of redox peaks appeared for the rGO/PANI composite electrode, which was attributed to the redox transitions of PANI (i.e., the leucoemeraldine/emeraldine transition). Therefore, the capacitance of rGO/PANI mainly comes from Faradaic reactions of PANI at the electrode/electrolyte surface,[29] which is different from that of the electric double-layer capacitance of carbon-based materials. Comparing the two curves, there is clearer symmetry in the redox peaks of PANI, especially at high scan rates, which indicates that both electron-transport and ion-diffusion rates in the rGO/PANI electrode are faster than that in the gold/PANI electrode. The Nyquist plots of rGO/PANI and gold/PANI electrodes are shown in Figure S4 in the Supporting Information. The almost-straight line in the low-frequency region demonstrates ideal capacitive behavior. In the high-frequency region, the plots show a semicircle that is related to the reduced electrical charge transfer resistance.

© 2012 WILEY-VCH Verlag GmbH & Co. KGaA, Weinheim

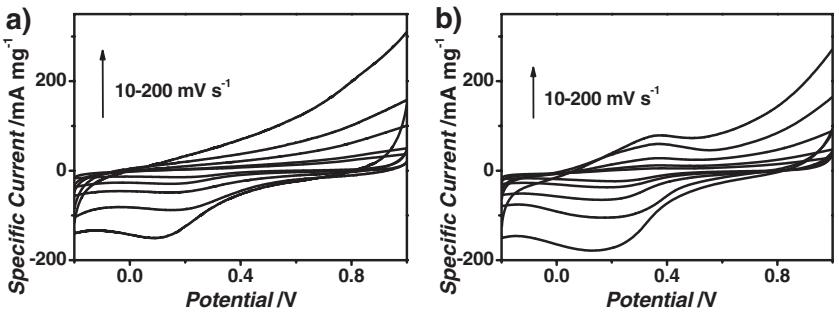

Figure 6. Comparison of CVs scanned from –0.2 to 1 V in 1 M Na_2SO_4 (aq) for the gold/PANI electrodes (a) and rGO/PANI composites electrodes (b) at scan rates of 10, 20, 50, 100, and 200 mV s^{-1} (from inner to outer).

From the Nyquist plots, it is clear that rGO/PANI showed low charge-transfer resistance.

To further confirm the merits of rGO/PANI composites as supercapacitor electrodes, the electrochemical properties of rGO, PANI, and rGO/PANI electrodes were fully characterized by galvanostatic charge/discharge and cycling-life measurement. The all-solid-state micro-supercapacitor (as shown in Figure S4a in the Supporting Information) is fabricated by coating H_3PO_4-polyvinyl alcohol (PVA) gel electrolyte on the rGO/PANI interdigital fingers. RGO and gold/PANI based all-solid-state micro-supercapacitors were fabricated in a similar way to obtain the electrochemical performances of rGO and PANI nanorod array electrodes. As the well-aligned PANI nanorods, nanocomposites of rGO/PANI show excellent performance as supercapacitor electrode materials. Above all, **Figure 7**a shows the galvanostatic charge/discharge curves of rGO, gold/PANI, and PANI nanorods in rGO/PANI composites at a current density of 2.5 A g^{-1} after calculating the relative value. The specific capacitances of rGO, PANI, and PANI nanorods in rGO/PANI composites are calculated according to the following equation:[1][a]

$$C_m = \frac{It}{\Delta V m}$$

where C_m is the specific capacitance (F g^{-1}), m is the mass of the active materials in the device (g), ΔV is 1 V, I is the charge/discharge current. The values are 155, 989.6, and 1268 F g^{-1}, respectively. Galvanostatic charge/discharge curves in Figure 7b show a capacitive behavior with almost symmetric curves of rGO/PANI composites at different current densities. The small deviation from linearity originates from the pseudocapacitive nature of PANI. Meanwhile, the deviation is not so clear for the synergistic effects of rGO and PANI. The nano scale of PANI nanorods may also be a factor in this.[1a,40] The specific capacitance of rGO/PANI is calculated as 973 F g^{-1} at a discharge current density of 2.5 A g^{-1}, which can be divided into two sections: the capacitance provided by rGO itself (the weight percentage of rGO within this composite is 26 wt%), and the specific capacitance of PANI nanorods within this composites. The high specific capacitance of rGO/PANI may contribute to the synergistic effect; PANI grows uniformly on rGO sheets and the vertically aligned PANI nanorods connect with rGO efficiently, which benefits the diffusion of ions from the bulky electrolyte to the surface of PANI nanorods. The counterions can thus reach or leave the surface of PANI nanowires fast. On the other hand, PANI nanorods with narrow diameters (ca. 20 nm) can shorten the charge-transport distance in the PANI materials. Thus, the counterions easily penetrate the inner layer of PANI, which makes nearly full use of the electrode materials. Combining the two factors, the ionic diffuse resistance and the charge-transfer resistance are reduced and the specific capacitance is substantially increased. So the synergistic effect between graphene and PANI plays an important role in improving the electrochemical properties of the composites. Despite the designed PANI nanorods on rGO patterns, random PANI nanorods were also constructed with high aniline concentration as well as long growth time. These random PANI nanorods were not fully used for energy storage, with much lower capacitance than aligned rGO/PANI nanocomposites, which is shown in Figure S5 in the Supporting Information. As shown in Figure 7c, the specific capacitance of rGO/PANI

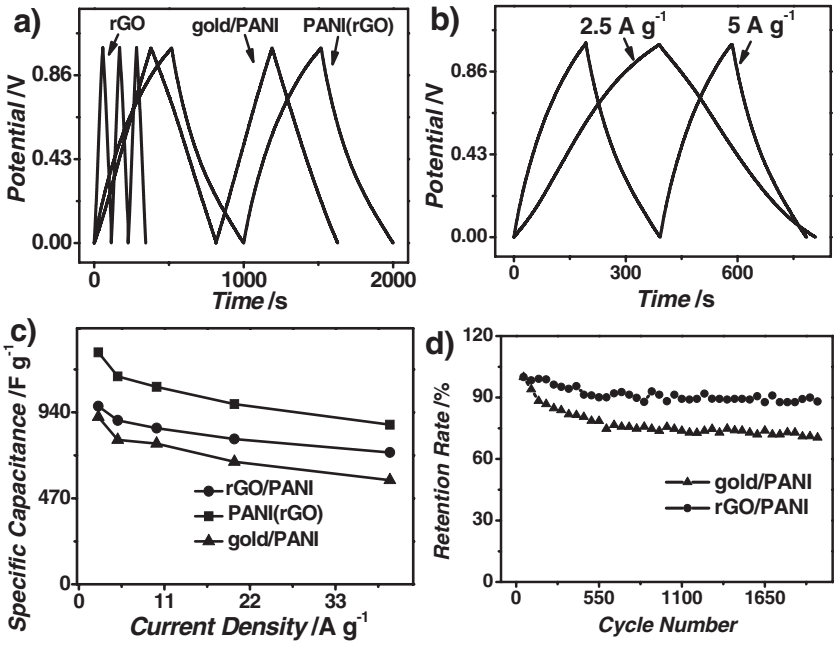

Figure 7. a) Galvanostatic charge/discharge curves of rGO, gold/PANI, and PANI nanorods in rGO/PANI (PANI(rGO)) at current density of 2.5 A g^{-1} after calculating the relative value. b) Galvanostatic charge/discharge curves of rGO/PANI with current densities of 2.5 and 5 A g^{-1}. c) Specific capacitance of gold/PANI (triangle), PANI in the rGO/PANI composites (square) and rGO/PANI (circle) based all-solid-state micro-supercapacitors at different charge/discharge current densities. d) Cycle stability of the all-solid-state devices at 2.5 A g^{-1} of the gold/PANI (triangle) and rGO/PANI (circle) based all-solid-state micro-supercapacitors. The high voltage of the test is 1 V.

© 2012 WILEY-VCH Verlag GmbH & Co. KGaA, Weinheim

composites decreases with increasing charge/discharge current densities. The specific capacitance of the composites is 970 F g^{-1} at a discharge current of 2.5 A g^{-1}, while it retains about 78% with growth of current densities from 2.5 to 40 A g^{-1}. Meanwhile, rGO/PANI composites possess much larger specific capacitance than gold/PANI in the current density range. This result suggests that rGO/PANI composites have good rate capability, which is very important for the electrode materials of a supercapacitor to provide high power density.

Generally speaking, conducting polymers as supercapacitor electrodes often suffer from limited long-term stability because the swelling and shrinking of the polymers may lead to degradation, which restricts these low-cost electrode materials for commercial application. However, the composition with rGO is able to meliorate this limit significantly. As shown in Figure 7d, the electrochemical stability of rGO/PANI was examined in the all-solid-state micro-supercapacitor by consecutive charge–discharge cycles at a current density of 2.5 A g^{-1}. rGO/PANI nanocomposites exhibited much higher stability than PANI nanorods on gold electrodes. For instance, after 1700 consecutive cycles, the rGO/PANI composites retained 90% of their initial capacitance, while gold/PANI decreased quickly to 80% after less than 500 cycles. The better stability of rGO/PANI composites may be ascribed to the synergistic effect of rGO and PANI nanorod arrays: Firstly, the vertical PANI nanorod arrays were susceptible to strain relaxation, which allowed them to reduce damage during the doping/dedoping process of counterions. Secondly, rGO nanosheets also can bear some mechanical deformation in the redox processes of the PANI nanorods, which avoids destruction of the electrode material and leads to greater stability. Thus, the rGO/PANI composites show enhanced cyclic stability over gold/PANI as supercapacitor electrode materials. Furthermore, the use of rGO and solid electrolyte are appealing for flexible electronics as it avoids the risk of harmful liquid leakage.

3. Conclusions

Well-ordered PANI nanorods on interdigital finger rGO electrodes were successfully grown in situ by electrochemical polymerization. Interdigital finger rGO electrodes were fabricated by MIMIC, and the morphologies of PANI nanorods could be controlled by the concentration of aniline and the growth time in the electrochemical process. These rGO/PANI composites were used to fabricate an all-solid-state flexible micro-supercapacitor that possesses electrochemical capacitance as high as 970 F g^{-1} at a discharge current density of 2.5 A g^{-1} and good stability that retains 90% of its initial capacitance after 1700 consecutive cycles. Our method may represent a route for translating the interesting fundamental properties of rGO and conducting polymers into technologically viable energy devices. This high-performance micro-supercapacitor provides a promising power source whose reliability and performance might help to meet the energy demands of the next generation of miniaturized electronic devices, especially flexible miniaturized electronic devices. Furthermore, this study will further guide the preparation of functional graphene-based materials.

4. Experimental Section

All materials and chemicals were purchased from Sinopharm Chemical Reagent Beijing and used as received. Conductance measurements were recorded on a Keithley 2400 sourcemeter. SEM images were recorded on a JEOL 7401 microscope. Optical images were recorded on a Nikon TE2000. Raman measurements were performed with a Renishaw Invia Raman Microscope spectrometer. The FTIR spectra were measured on an FTIR 8400S spectrophotometer (Shimadzu, Japan). All electrochemical measurements were conducted with a computer-controlled CHI660B electrochemical analyzer (CH Instruments, Shanghai Chenhua Instrument Corporation, China). Specific surface areas of the rGO were determined using a Micromeritics ASAP-2010 instrument at liquid-nitrogen temperature.

Fabrication of Patterned rGO Electrodes: GO sheets were synthesized by a modified Hummer method[41] using natural graphite powder. The GO aqueous solution was fabricated by dispersing the GO sheets in water after a two-step sonication, as follows: GO was mildly sonicated for 2 h to achieve a stable aqueous suspension. Strong sonication was then applied to the suspension for 20 min to break up the large GO sheets. The resulting GO solution was then centrifuged at 1500 rpm for 2 h, after which the mixture separated into two phases. The upper phase was collected to remove the larger GO sheets, and then centrifuged at 10 000 rpm for 2 h to remove the smaller GO sheets (diameter <300 nm). The lower phase was collected and used for GO patterning.

Soft lithography and rapid prototyping were used to fabricate features in SU-8 (Microchem) that were subsequently replica molded using PDMS prepolymer to fabricate the flexible stamps. Prior to rGO patterning, the flat side of the PDMS stamp was treated with O_2 plasma for 10 min. Then the flat PDMS stamp and a patterned PDMS stamp as shown in Figure 1 were put together with a weight on the top to give conformal contact. A drop of GO aqueous solution (≈1 mg mL^{-1}) was then placed at each end of the PDMS stamp. After heating under vacuum with hydrazine solution and then degassing for 30 min at room temperature, the whole system was then warmed to 70 °C (at a heating rate of 5 °C min^{-1}), which was maintained for 12 h to obtain patterned rGO electrodes. The resulting rGO patterns on the PDMS stamp were characterized by optical microscopy, micro-Raman spectroscopy and AFM. AFM images were obtained in tapping mode with an Si tip under ambient conditions, a scanning rate of 1 Hz, and a scanning line of 512. Raman spectra were recorded using micro-Raman spectroscopy with excitation wavelength at 532 nm to monitor the surface composition of the rGO. Linear *I–V* curves were recorded on a Keithley 2400 sourcemeter at potential from –1 to 1 V on rGO electrodes.

Electrochemical Growth of PANI Nanorod Arrays on rGO and Gold Interdigital Finger Electrodes: A fresh PDMS stamp was evaporated with 20 nm Au and 2 nm Ti through magnet sputtering. Both the metal-coated stamp and another piece of freshly peeled flat PDMS slab were plasma treated for 1 min, and then brought into conformal contact. After the separation, a complete transfer of the metal pattern from the raised regions of the stamp to the plasma-treated PDMS was made. The rGO electrodes and gold electrodes were used directly as the working electrode in a three-electrode configuration that was constructed with a Pt plate as counter electrode and Ag/AgCl as reference electrode. The electrolyte was H_2SO_4 (0.5 mol L^{-1}) and aniline (0.05 mol L^{-1}). PANI was electropolymerized on the electrodes at a constant potential of 0.75 V versus reference electrode for various periods (1000, 2000, 4500, 5000, and 10 000 s). After electrochemical growth, the PANI nanorod arrays were washed with distilled water and dried. Raman spectra with the excitation wavelength at 532 nm were used to study the electrochemical growth of PANI nanorod arrays on the rGO surface. The resulting rGO/PANI composites and the gold/PANI were characterized by SEM and FTIR.

Fabrication and Electrochemical Measurements of All-Solid-State Micro-Supercapacitors: The gold/PANI and rGO/PANI composites were used directly as working electrode in a three-electrode test cell with Na_2SO_4 (1 mol L^{-1}) as electrolyte, Ag/AgCl electrode as reference electrode, and Pt plate as counter electrode. All working electrodes were weighed after

© 2012 WILEY-VCH Verlag GmbH & Co. KGaA, Weinheim

careful washing and then drying at 70 °C for 24 h. The weight of the rGO/PANI electrode for electrochemical test is ≈5.50 mg. The CVs were collected on a computer-controlled CHI660B electrochemical analyzer from 10 to 200 mV s^{-1}. The CV potential range was from –0.2 to 1 V. The H_3PO_4- PVA gel electrolyte was then prepared as follows: PVA powder (10.0 g) was added to deionized water (100 mL) and then heated steadily to ≈85 °C with vigorous stirring until the solution became clear. After cooling, H_3PO_4 (8.0 g) was added, and the mixture was heated to partial dryness at 35 °C for 6 h. The rGO/PANI composites with patterns were cut from the dashed line (as shown in Figure 1, with 2×5 cm^2 left) to obtain the interdigital fingers. Both sides of the interdigital fingers were attached by aluminum conducting tape and then H_3PO_4- PVA gel electrolyte was used to coat the tapes. The all-solid-state micro-supercapacitor was complete when the electrolyte was dry and the aluminum conducting tapes could be easily wired into external circuitry. rGO and gold/PANI based all-solid-state micro-supercapacitors were fabricated in a similar way. All electrochemical measurements were carried out at room temperature. Galvanostatic charge/discharge measurements were used to accurately evaluate the electrochemical performance of the devices. Various current densities (2.5 to 40 A g^{-1}) were applied, and a current density of 2.5 A g^{-1} was used for the cycling life tests.

Supporting Information

Supporting Information is available from the Wiley Online Library or from the author.

Acknowledgements

This investigation was supported by the Natural Science Foundation of China (grant Nos. 20733001 and 91027029), the Fundamental Research Funds for the Central Universities and the Research Funds of Renmin University of China (grant No. 10XNI005). We would like to thank Dr. Zhibo Li at Beijing National Laboratory for Molecular Sciences (BNLMS) for providing funding support.

Received: August 23, 2011
Revised: October 25, 2011
Published online: January 19, 2012

[1] a) Y. G. Wang, H. Q. Li, Y. Y. Xia, *Adv. Mater.* **2006**, *18*, 2619; b) W. Gao, N. Singh, L. Song, Z. Liu, A. L. M. Reddy, L. Ci, R. Vajtai, Q. Zhang, B. Wei, P. M. Ajayan, *Nat. Nanotech.* **2011**, *6*, 496; c) L. Q. Mai, F. Yang, Y. L. Zhao, X. Xu, L. Xu, Y. Z. Luo, *Nat. Commun.* **2011**, *2*, 381; d) Y. Zhu, S. Murali, M. D. Stoller, K. J. Ganesh, W. Cai, P. J. Ferreira, A. Pirkle, R. M. Wallace, K. A. Cychosz, M. Thommes, D. Su, E. A. Stach, R. S. Ruoff, *Science* **2011**, *332*,1537; e) Y. F. Yan, Q. L. Cheng, G. C. Wang, C. Z. Li, *J. Power Sources* **2011**, *196*, 7835.
[2] L. Song, A. Zhamu, J. Guo, B. Z. Jang, *US Patent,* **2006**, *US 7623340 B1*.
[3] a) X. Zhou, X. Huang, X. Qi, S. Wu, C. Xue, F. Y. C. Boey, Q. Yan, P. Chen, H. Zhang, *J. Phys. Chem. C* **2009**, *113*, 10842; b) S. Gilje, S. Han, M. Wang, K. L. Wang, R. B. Kaner, *Nano Lett.* **2007**, *7*, 3394.
[4] H. Gómez, M. K. Ram, F. Alvi, P. Villalba, E. Stefanakos, A. Kumar, *J. Power Sources* **2011**, *196*, 4102.
[5] Z. Yin, S. Wu, X. Zhou, X. Huang, Q. Zhang, F. Boey, H. Zhang, *Small* **2010**, *6*, 307.
[6] K. S. Kim, Y. Zhao, H. Jang, S. Y. Lee, J. M. Kim, K. S. Kim, J.-H. Ahn, P. Kim, J.-Y. Choi, B. H. Hong, *Nature* **2009**, *457*, 706.
[7] C. Berger, Z. M. Song, X. B. Li, X. S. Wu, N. Brown, C. Naud, D. Mayou, T. B. Li, J. Hass, A. N. Marchenkov, E. H. Conrad, P. N. First, W. A. de Heer, *Science* **2006**, *312*, 1191.
[8] C. Gomez-Navarro, R. T. Weitz, A. M. Bittner, M. Scolari, A. Mews, M. Burghard, K. Kern, *Nano Lett.* **2007**, *7*, 3499.
[9] C. N. R. Rao, A. K. Sood, K. S. Subrahmanyam, A. Govindaraj, *Angew. Chem. Int. Ed.* **2009**, *48*, 7752.
[10] M. Ishigami, J. H. Chen, W. G. Cullen, M. S. Fuhrer, E. D. Williams, *Nano Lett.* **2007**, *7*, 1643.
[11] X. Wang, L. Zhi, K. Müllen, *Nano Lett.* **2007**, *8*, 323.
[12] E. J. Yoo, J. Kim, E. Hosono, H. S. Zhou, T. Kudo, I. Honma, *Nano Lett.* **2008**, *8*, 2277.
[13] J. R. Miller, R. A. Outlaw, B. C. Holloway, *Science* **2010**, *329*, 1637.
[14] Y. Wang, Z. Q. Shi, Y. Huang, Y. F. Ma, C. Y. Wang, M. M. Chen, Y. S. Chen, *J. Phys. Chem. C* **2009**, *113*, 13103.
[15] M. D. Stoller, S. Park, Y. W. Zhu, J. An, R. S. Ruoff, *Nano Lett.* **2008**, *8*, 3498.
[16] H. L. Wang, Q. L. Hao, X. J. Yang, L. D. Lu, X. Wang, *Electrochem. Commun.* **2009**, *11*, 1158.
[17] C. Liu, Z. Yu, D. Neff, A. Zhamu, B. Z. Jang, *Nano Lett.* **2010**, *10*, 4863.
[18] T. Y. Kim, H. W. Lee, M. Stoller, D. R. Dreyer, C. W. Bielawski, R. S. Ruoff, K. S. Suh, *ACS Nano* **2011**, *5*, 436.
[19] A. Rudge, J. Davey, I. Raistrick, S. Gottesfeld, *J. Power Sources* **1994**, *47*, 89.
[20] G. Y. Zhao, H. L. Li, *Microporous Mesoporous Mater.* **2008**, *110*, 590.
[21] V. Gupta, N. Miura, *Electrochem. Solid-State Lett.* **2005**, *8*, A630.
[22] J. Y. Huang, K. Wang, Z. X. Wei, *J. Mater. Chem.* **2010**, *20*, 1117.
[23] K. Wang, J. Y. Huang, Z. X. Wei, *J. Phys. Chem. C* **2010**, *114*, 8062.
[24] H. Zhang, G. P. Cao, Z. Y. Wang, Y. S. Yang, Z. J. Shi, Z. N. Gu, *Eletrochem. Commun.* **2008**, *10*, 1056.
[25] H. Zhang, G. P. Cao, W. K. Wang, K. G. Yuan, B. Xu, W. F. Zhang, J. Cheng, Y. S. Yang, *Electrochim. Acta* **2009**, *54*, 1153.
[26] P. J. Hung, K. H. Chang, Y. F. Lee, C. C. Hu, K. M. Lin, *Electrochim. Acta* **2010**, *55*, 6015.
[27] A. V. Murugan, T. Muraliganth, A. Manthiram, *Chem. Mater.* **2009**, *21*, 5004.
[28] D. W. Wang, F. Li, J. Zhao, W. Ren, Z. G. Chen, J. Tan, Z. S. Wu, I. Gentle, G. Q. Lu, H. M. Cheng, *ACS Nano* **2009**, *3*, 1745.
[29] J. J. Xu, K. Wang, S. Z. Zu, B. H. Han, Z. X. Wei, *ACS Nano* **2010**, *4*, 5019.
[30] a) J. Yan, T. Wei, B. Shao, Z. J. Fan, W. Z. Qian, M. L. Zhang, F. Wei, *Carbon* **2010**, *48*, 487; b) C. Z. Meng, C. H. Liu, L. Z. Chen, C. H. Hu, S. S. Fan, *Nano Lett.* **2010**, *10*, 4025; c) K. Zhang, L. L. Zhang, X. S. Zhao, J. S. Wu, *Chem. Mater.* **2010**, *22*, 1392.
[31] E. Kim, Y. N. Xia, G. M. Whitesides, *J. Am. Chem. Soc.* **1996**, *118*, 5722.
[32] Z. Yin, S. Wu, X. Zhou, X. Huang, Q. Zhang, F. Boey, H. Zhang, *Small* **2010**, *6*, 307.
[33] Q. He, H. G. Sudibya, Z. Yin, S. Wu, H. Li, F. Boey, W. Huang, P. Chen, H. Zhang, *ACS Nano* **2010**, *4*, 3201.
[34] A. B. Kaiser, C. Gomez-Navarro, R. S. Sundaram, M. Burghard, K. Kern, *Nano Lett.* **2009**, *9*, 1787.
[35] Y. L. Loo, R. L. Willett, K. W. Baldwin, J. A. Rogers, *J. Am. Chem. Soc.* **2002**, *124*, 7654.
[36] L. Z. Fan, Y. S. Hu, J. Maier, P. Adelhelm, B. Smarsly, M. Antonietti, *Adv. Funct. Mater.* **2007**, *17*, 3083.
[37] a) H. L. Wang, Q. L. Hao, X. J. Yang, L. D. Lu, X. Wang, *Nanoscale* **2010**, *2*, 2164; W. R. Li, D. H. Chen, Z. Li, Y. F. Shi, Y. Wan, G. Wang, Z. Y. Jiang, D. Y. Zhao, *Carbon* **2007**, *45*, 1757.
[38] a) M. C. Bernard, A. H. Goff, *Electrochim. Acta* **2006**, *52*, 595; b) M. C. Bernard, A. H. Goff, H. Arkoub, B. Saidani, *Electrochim. Acta* **2007**, *52*, 5030.
[39] M. C. Bernard, A. H. Goff, *Electrochim. Acta* **2006**, *52*, 728.
[40] a) H. L. Wang, Q. L. Hao, X. J. Yang, L. D. Lu, X. Wang, *Appl. Mater. Interfaces* **2010**, *2*, 821; b) X. B. Yan, J. T. Chen, J. Yang, Q. J. Xue, P. Miele, *Appl. Mater. Interfaces* **2010**, *2*, 2521.
[41] W. S. Hummers, R. E. Offeman, *J. Am. Chem. Soc.* **1958**, *80*, 1339.

© 2012 WILEY-VCH Verlag GmbH & Co. KGaA, Weinheim